Surface oxygen versus native oxide on tungsten: contrasting effects on deuterium retention and release

Axel Dunand, Marco Minissale, Jean-Bernard Faure, Laurent Gallais, Thierry Angot, R. Bisson

https://doi.org/10.1088/1741-4326/ac583a

Surface oxygen versus native oxide on tungsten: contrasting effects on deuterium retention and release

A. Dunand[1], M. Minissale[1], J.-B. Faure[1], L. Gallais[2], T. Angot[1], and R. Bisson[1]

[1]Aix-Marseille Univ, CNRS, PIIM, UMR 7345, Marseille, France

[2]Aix-Marseille Univ, CNRS, Centrale Marseille, Institut Fresnel, Marseille, France

Email:
axel.dunand@univ-amu.fr ; regis.bisson@univ-amu.fr

Abstract

We performed a direct comparison of deuterium retention and release from tungsten in presence or in absence of oxygen impurities. A single crystal of W(110) was used to prepare tungsten with four different surface states: with its native oxide, atomically clean, covered with half a monolayer of oxygen atoms, and covered with three fourths of a monolayer of oxygen atoms. For a D ion fluence of 3×10^{21} D^+ m^{-2} implanted at 300 K, deuterium retention was highest with the native oxide, lowest with three fourths of a monolayer of oxygen atoms at the surface and intermediate for the clean surface. This counterintuitive result is explained by a different localization of deuterium retention in these samples. For tungsten with its native oxide, deuterium retention occurs solely in the bulk, i.e. below the first atomic plane of the surface. For clean tungsten, deuterium retention occurs in part at the surface and sputtering should play a role. For tungsten with a sub-monolayer surface coverage of oxygen atoms, a transition from surface to bulk retention is observed above half a monolayer of adsorbed oxygen. Striking differences in desorption peak(s) temperature(s) are observed between D ion-implanted samples and D_2 molecules-exposed samples. These results highlight the importance of the (near-) surface localization of oxygen and deuterium on the temperature dependence of deuterium desorption rate i.e. on the fusion fuel recycling coefficient.

Keywords: tungsten, oxygen, deuterium, retention, bulk, surface, fuel recycling

Introduction

In ITER and in future fusion reactors such as DEMO, tungsten (W) will be an important plasma facing material as it will constitute, respectively, the divertor exhaust targets and the tokamak first walls. A detailed understanding of the interaction of W with the fusion products (helium and neutron) and the fusion fuel (deuterium (D) and tritium) is needed, especially because tritium is a scarce and radioactive element. Tungsten exposure to fusion products generate morphology changes in the bulk of W, as numerous studies have shown [1–4], and the influence of such bulk defects onto fusion fuel retention is presently an active field of research [5,6]. In contrast, pure surface effects are often neglected in plasma-wall interaction studies and global recycling coefficients are used for simulating edge plasma physics [7]. However, recent experiments highlighted that the surface of W may play a significant role in bulk retention of hydrogen isotopes. ‘t Hoen et al. have performed high flux (10^{24} m^{-2} s^{-1}) low energy D implantation in self-damaged polycrystalline W and found that the effective bulk penetration flux was much smaller for 5 eV implantation than for 40 eV implantation [8]. They argued that the high D flux would remove the native oxygen and carbon impurities of W and thus a protective chemisorbed surface layer of D would act as a bulk penetration barrier for 5 eV incident D. Nevertheless, the argument of plasma removal of surface impurities was not supported by *in situ* measurements of the surface elemental composition.

Such carbon and oxygen impurities are however a possible source of hydrogen isotope trapping in the bulk, i.e. below the

https://doi.org/10.1088/1741-4326/ac583a

first atomic plane of the surface, as it has been shown in density function theory (DFT) studies [9]. We recently demonstrated [10] that the DFT energetics for D detrapping from these impurities can explain partly the dynamic D retention observed in laboratory experiments for W poly-crystals [11] and single crystals [12]. In these studies, we argued that the < 5 nm native oxide of W should be considered as a trapping layer for the fusion fuel that influences retention measurements by temperature programmed desorption (TPD) and nuclear reaction analysis (NRA). This argument was recently supported by the work of Kremer et al. [13] who showed that relatively thin (30-50 nm) WO_3 oxides efficiently retain D, consistent with previous experiments performed on thick (> 100 nm) WO_3 oxides [14,15].

The aim of the present study was three-fold. First, we sought to clarify the role of the native oxide in the trapping of hydrogen isotope in W. Second, we wanted to understand the behavior of a bulk defect-free and clean W surface in terms of hydrogen isotope retention. Finally, we intended to study the behavior of pure crystalline oxygen surface layers under hydrogen isotope ion implantation. These last two goals should offer well-defined experimental data amenable for quantitative DFT and kinetic modeling.

Experimental methods

Experiments presented here were realized in the Advanced MUltibeam experiment for Plasma Surface Interaction (AMU-PSI), an ultra-high vacuum (UHV) setup recently commissioned at Aix-Marseille University (Marseille, France) [16]. In this study, we used two of the multiple interconnected chambers: the sample chamber (base pressure $P \approx 2\times10^{-8}$ Pa) and the ion beam/mass spectrometer chamber (base pressure $P \approx 5\times10^{-8}$ Pa). In the sample chamber, the W sample is mounted on a molybdenum plate attached to a 4-axis manipulator. The sample temperature is measured on the implanted face with a mechanically-pressed C-type thermocouple and is controlled by a computer-based PID regulator. The sample is a cylindrical (8 mm diameter, 2 mm thick) pure (99.999%) W single crystal oriented along the (110) crystallographic plane. The W(110) sample was aligned and mechanically polished with an accuracy of 0.1°. The W sample is heated either with a tungsten filament (up to ~1000 K) or with a CW Ytterbium fiber laser (SPI laser Qube 1000) delivering up to 1000 W at ~1075 nm. Filament heating was used for temperature programmed desorption (TPD) measurements and laser heating was used both to remove impurities from the sample and to grow well-defined oxygen coverage on the sample surface. A leak valve allows to set a pressure of oxygen in the sample chamber. A four-grid low-energy electron diffractometer (LEED)/Auger electron spectrometer (AES) (OCI BDL600IR) complement the sample chamber and is used to characterize the crystalline structure and the chemical composition of the sample surface at room temperature. In the ion beam/mass spectrometer chamber, a commercial ion source (FOCUS FDG150) is used to produce a D_2^+ ion beam with a kinetic energy of 250eV/D and a flux of 0.5×10^{18} D_2^+ m^{-2} s^{-1}. The ion beam impinges the sample normal to its surface and the ion beam footprint was measured by LEED on crystalline oxidized W(110) to be ~ 6.5 mm in diameter. We quantified the release of hydrogen isotopes from the sample during TPD using a quadrupole mass spectrometer (QMS) (MKS Microvision2).

As received and after a first annealing to 1200 K for 210 seconds, to remove physisorbed impurities such as water and hydrocarbons, the sample is covered by a native oxide with thickness less than 5 nm that cannot be resolved by focused ion beam scanning electron microscopy [10]. We confirmed the 5 nm thickness limit of a W native oxide using angle-resolved X-ray photoelectron spectroscopy in the Nautilus apparatus (Marseille, France) [17] (not shown). Figure 1.left presents LEED measurements of the W(110) sample with its native oxide that exhibit an inhomogeneous surface: amorphous domains, related to the greyish background, are superimposed with diffraction spots which patterns inform on the presence of crystalline impurities over-layers.

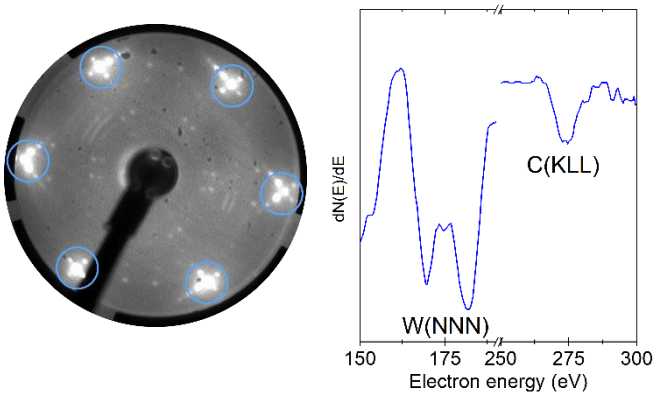

Figure 1. (left) LEED measurements (electron beam energy of 80 eV) of a "native oxide" on W(110) annealed to 1200 K . Blue circles indicate the location of the diffraction spots of the W(110) surface lattice. (right) AES measurements (derivative mode, electron beam energy of 1.5 keV) of the "native oxide" annealed to 2200 K. The electron beam probe dimension is ~0.25 mm.

The chemical nature of these impurities is determined with AES (Figure 1.right). Apart the signatures of oxygen at 503 eV (O(KLL), not shown, see [10]) and tungsten at 169 and 179 eV (W(NNN)), an Auger peak at 272 eV characteristic of carbon impurities (C(KLL)) is detected all over the sample. Upon high temperature annealing (> 1600 K), we found that some areas of the sample have more contrasted and sharper LEED diffractograms and coincides spatially with the strong Auger peak at 272 eV, suggesting carbon segregation at the W surface. Thus, the "native oxide" of W is actually chemically and structurally inhomogeneous, justifying the use of quotation marks from now on.

https://doi.org/10.1088/1741-4326/ac583a

The clean W(110) surface was obtained with a method inspired by Zakeri *et al.* [18]. Consecutive laser shots lasting 5 s at 300 W and repeated every 5 min brought temporarily the sample temperature to 1873 K in an O_2 atmosphere ($P(O_2)$ = 1×10^{-5} Pa). This oxidative step removes the carbon segregated on the sample surface by production of CO molecules. Then, heating the sample to >2200 K (650 W) allows the desorption of oxygen atoms. This method was repeated about 500 times to achieve an atomically clean W(110) sample without any carbon or oxygen impurities as demonstrated with LEED and AES (Figure 2).

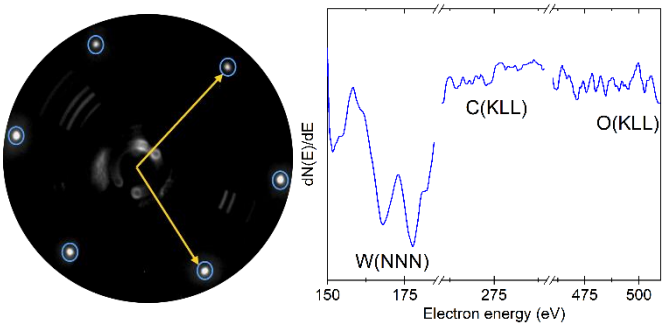

Figure 2. (left) LEED measurement (80 eV) of the clean W(110) sample. Blue circles indicate the location of the diffraction spots of the W(110) surface lattice and yellow arrows represent reciprocal lattice vectors. (right) AES measurements of the clean W(110) sample.

Pure crystalline oxygen layers were selected based on their consistent description in the literature [19–21] and were grown *in situ* from clean W(110). The first selected oxygen layer is the W(110):O-p(2×1) ($O_{0.50ML}$ surface in the following) which is defined by an oxygen coverage of 0.50 monolayer where an oxygen atoms row (diagonal row of red circles in Figure 3.left) is present every two tungsten atoms rows (blue circles). One monolayer (ML) is the W(110) surface atom density of 1.42×10^{19} m^{-2} [22]. The second selected oxygen layer is the W(110):O-p(2×2) ($O_{0.75ML}$ surface in the following) which is defined by an oxygen coverage of 0.75 ML where a second oxygen atoms row with half density is added to the $O_{0.50ML}$ surface (Figure 3.right). Note that in contrast to the literature, we did not use an exposure of a clean W(110) to O_2 pressure at room temperature followed by a sample annealing, but an O_2 exposure ($P(O_2)$ = 1×10^{-5} Pa) on the clean W(110) as it cools down. The advantage of our method is to reduce the duration of the preparation for the O-p(2×1) and O-p(2×2) layers by a factor of 2 while achieving sharper LEED patterns indicating larger domains of the desired crystalline structures. Deuterium implantation was performed on prepared W(110) only when the desired crystalline structure were confirmed by LEED and once the sample temperature was at 300 K. A fluence of 3×10^{21} D^+ m^{-2} was systematically realized by time integration of the measured ionic current on the sample. Note that during D_2^+ ion implantation, the D_2 pressure in the ion beam/mass spectrometer chamber was 2×10^{-5} Pa creating a pressure rise in the sample chamber to 1×10^{-6} Pa. Thus, concurrent to the ion flux of 0.5×10^{18} D_2^+ m^{-2} s^{-1}, there is a thermal molecular neutral flux of 4.3×10^{18} D_2 m^{-2} s^{-1} on the sample coming from the ion beam/mass spectrometer chamber. This neutral flux alone is sufficient to saturate the W(110) surface during the timed exposure of the present experiments (not shown) and it will be accounted for in the following. After implantation, one waited 1 hour to allow a sufficient reduction of the D_2 partial pressure in the ion beam/mass spectrometer chamber. Approximatively midway during D implantation, the $O_{0.50ML}$ and $O_{0.75ML}$ surfaces became amorphous as measured by LEED (not shown). Nevertheless, the oxygen coverage remained high since these D-implanted oxygen surfaces adopted a crystalline 337-phase superstructure [23] after the realization of the TPD. This observation is consistent with the absence of detection of heavy water during TPD. Thus, D retention was evaluated by adding the hydrogen isotopes desorption flux at m/z = 3 and 4 (for HD and D_2, respectively) during a temperature ramp of 5 $K\ s^{-1}$ up to 1000 K, and are shown as TPD traces.

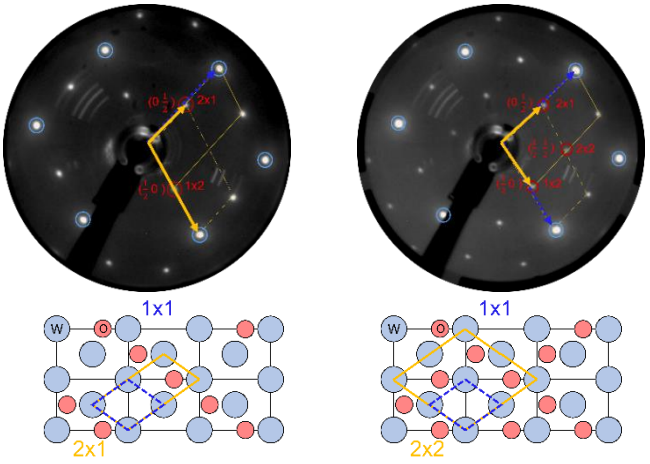

Figure 3. (top left) LEED measurement (110 eV) of the W(110):O-p(2×1) surface. (bottom left) top-view model of the corresponding W surface with 0.50 ML of adsorbed oxygen ($O_{0.50ML}$). (top right) LEED measurement of the W(110):O-p(2×2) surface. (bottom right) model of the corresponding W surface with 0.75 ML of adsorbed oxygen ($O_{0.75ML}$).

Results and discussion

Figure 4 presents the TPD obtained for an identical D ion fluence implanted at 300 K onto the four distinct surfaces introduced previously. D retention is found to be the highest for the W surface with the inhomogeneous "native oxide" and the lowest for the $O_{0.75ML}$ surface. D retention for the $O_{0.50ML}$ surface is slightly higher than for the $O_{0.75ML}$ surface. Finally, the clean W(110) sample exhibits a D retention intermediate

https://doi.org/10.1088/1741-4326/ac583a

between the "native oxide" and the $O_{0.50ML}$ surface. The four TPD spectra display similar shape and width with a single maximum located at 400±5 K and a desorption visible up to 600 – 650 K.

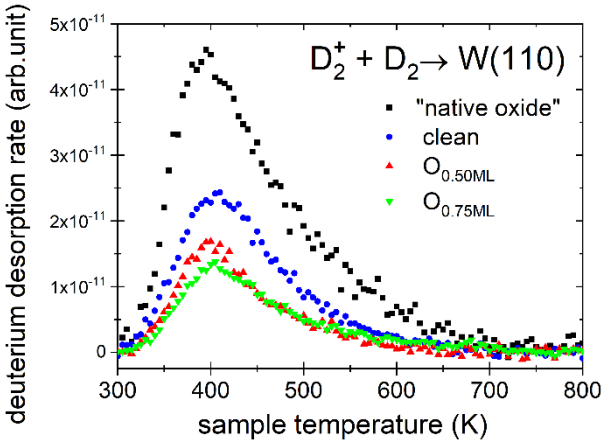

Figure 4: TPD measurements after a D_2^+ ion implantation of 3×10^{21} D m^{-2} at 300 K *onto a W(110) with its "native oxide" (black square), a clean W(110) (blue circle), a W(110):O-p(2×1) surface (red up-triangle) and a W(110):O-p(2×2) surface (green down-triangle). The ion flux (*0.5×10^{18} D_2^+ m^{-2} s^{-1}*) is concomitant with a molecular flux (*4.3×10^{18} D_2 m^{-2} s^{-1}*).*

We recall that in the present experiment a molecular flux is concurrent with the ionic flux during D ion implantation. Dissociative adsorption of molecular D_2 is expected on the clean surface of W(110) [22] as well as on the surface of oxidized W in the sub-monolayer regime [24]. Thus, in order to disentangle bulk D absorption from surface D adsorption, we performed TPD measurements following an exposure to pure molecular D_2 (Figure 5), with identical time and sample chamber pressure conditions as for an ion implantation.

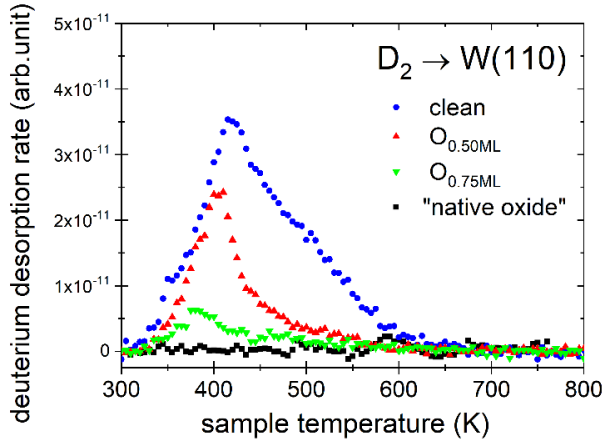

Figure 5: TPD measurements following molecular D_2 exposure (300 K, same time and flux than in Figure 4) onto a W(110) with its "native oxide" (black square), a clean W(110) (blue circle), a W(110):O-p(2×1) surface (red up-triangle) and a W(110):O-p(2×2) surface (green down-triangle).

Following molecular D_2 exposure, D retention on the surface of clean W(110) is the highest, followed by the $O_{0.50ML}$ surface and the $O_{0.75ML}$ surface, while the "native oxide" does not retain deuterium on its surface. The TPD spectra shape and width is markedly different for D adsorbed on the surface of W(110) as compared for D implanted in W(110). For the clean W(110) exposed to molecular D_2, the TPD presents two desorption peaks at 415 K and 500 K. For the $O_{0.50ML}$ and $O_{0.75ML}$ surfaces, as the oxygen coverage increases, the 500 K desorption peak vanishes while the 415 K desorption peak shifts to 400 K and then 380 K, and its height strongly decreases. All these results for D_2 exposure of clean and oxygen covered W(110) are consistent with Tamm and Schmidt [22] and Whitten and Gomer [24] results.

Having determined how much D retention can be expected in our experimental conditions from the surface of the present W(110) sample, we subtracted the D retention obtained after D_2 molecular exposure (Figure 5) from the D retention obtained after D ion implantation (Figure 4), in an attempt to estimate the share of D retention between the bulk and the surface of W (Figure 6).

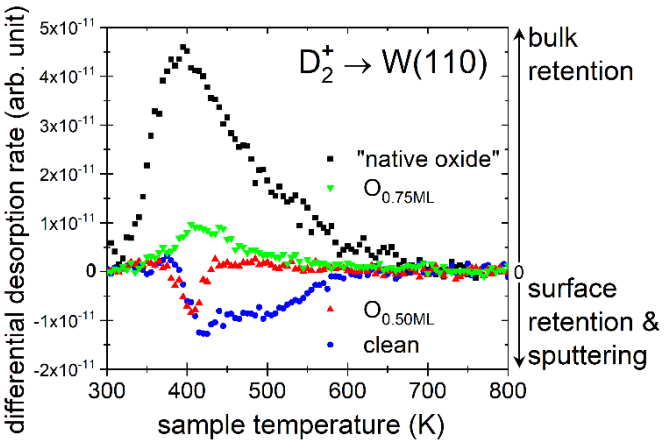

Figure 6: Subtraction of TPD measurements of Figure 5 (D_2 molecular exposure) from Figure 4 (D_2^+ ion implantation concomitant with D_2 molecular exposure) to highlight various contributions to deuterium retention during D ion implantation.

Rigorously, subtracting the data of Figure 5 (molecular exposure) from the data of Figure 4 (ion implantation + molecular exposure) should highlight both the effect of D surface retention and the effect of sputtering of D adsorbed at the surface by impinging D ions. Therefore, apart for the "native oxide" where there is clearly no D adsorption (black squares in Figure 5), the extent of D surface retention for clean and sub-monolayer oxygen surface coverage cannot be estimated directly from Figure 6; this is due to the opposing effects of D surface retention from D_2 molecular exposure and D_2+ ions sputtering of adsorbed D. Nonetheless with this precaution in mind, Figure 6 shows that the "native oxide" retains implanted D ions only in its bulk, i.e. below the first

atomic plane of the surface, while a significant part of D retention is retained in the bulk of the $O_{0.75ML}$ sample. In contrast, both the $O_{0.50ML}$ and the clean surfaces of W(110) display a negative differential retention, i.e. a higher retention is obtained for molecular exposure alone, which indicates that surface microscopic events play a significant role in the overall retention after ion implantation through the equilibrium between D adsorption and D ions sputtering of adsorbed D.

To summarize the present results, we observed that the total retention of D in W decreases when the surface oxygen coverage increases, if one stays in the sub-monolayer regime of the pure oxygen overlayer. In this case, the role of the surface is important through the competition between the adsorption of D at the surface and its subsequent sputtering by impinging D ion. However, for an oxide that is thicker than a monolayer and contains carbon (i.e. the "native oxide"), the retention of D is increased significantly, with respect to the clean surface in the present fluence range, and D retention occurs solely in the bulk of W. We shall know discuss the implication of these results.

First, the highest D retention observed for the “native oxide” should be related to its thickness and inhomogeneous (i.e. defective) nature. We previously modeled such layer [10] using a simple proxy based on DFT studies for impurity-single vacancy complex [9]. However, we have shown presently that the “native oxide” contains various crystalline and amorphous domains. Future studies should focus on the growth of thicker (i.e. a few monolayer) pure oxides (or carbides) to estimate separately the role of oxygen (or carbon) impurities in D retention. Such results should help to rationalize the effect of the “native oxide” on TPD and NRA measurements in laboratory studies and it may also be useful to estimate the role of natural impurities in D retention in W plasma facing components.

Second, the decrease in D retention when increasing the oxygen sub-monolayer coverage, both for D-implanted W and D_2-exposed W, can be explained by the decrease in available site for the adsorption of D on the W surface when the O coverage increases. DFT studies have shown that D [25,26] adsorbs on the same three-fold hollow site of the W(110) surface than O [27], indeed. Therefore, a small amount of oxygen impurities in the particles flux at the divertor surface could lead to a significant reduction of D adsorption on W and thus reduce the protective nature of the chemisorbed surface layer discussed by ‘t Hoen et al. for ITER-like D ion flux [8]. Such oxygen coverage effect in ITER should be factored in with the local temperature of tungsten. Considering the second order desorption kinetics of deuterium from clean W(110) characterized by Tamm and Schmidt [22], one should expect that the desorption flux would be on par with ITER’s hydrogen isotopes impinging flux (~10^{24} $m^{-2}s^{-1}$) between 800 and 1000 K, thus the protective chemisorbed layer maybe present on a clean divertor. In presence of oxygen however, considering the shift of desorption peaks observed in our TPD and in the ones of Whitten and Gomer [24], one should expect that the desorption flux would be on par with ITER’s hydrogen isotope impinging flux between 600 and 800 K, i.e. the protective chemisorbed layer could be absent at ITER strike lines in presence of oxygen contamination.

Third, when the W surface is totally covered with site-blocking impurities (as with the native oxide) and there are no grain boundaries (as in a single crystal), where does the deuterium recombination takes place to release D_2 and HD? Additional DFT studies are needed to clarify the actual mechanistic steps that lead to the release of hydrogen isotopes from W which cannot adsorb dissociatively D_2 on its surface, like for the “native oxide” of W. This recombinative desorption mechanism conundrum may be understood by studying further the differences in TPD shapes for D-implanted W versus D_2-exposed W. As one can observe by comparison of Figure 4 and 5, which have been obtained on the very same samples but with different deuterium sources, such differences in TPD shapes demonstrate that the kinetics of hydrogen isotope release is affected by the spatial origin of D atoms. On the one hand, hydrogen isotope molecules produced by recombination of two adsorbed D atoms exhibits two desorption peaks which temperature of maximum desorption rate is strongly influenced by surface impurities (Figure 5). On the other hand, hydrogen isotope molecules produced through a resurfacing step (i.e. at least one of the D atom is coming from the bulk) shows a single desorption peak which temperature is unaffected by the surface composition (Figure 4). These results call for the development of DFT-based kinetic models that would include the details of the minimum energy paths for D atoms diffusing from the bulk to the surface. Such macroscopic rate equations model could describe more accurately the release of hydrogen isotopes observed in laboratory measurements. Finally, a detailed description of the hydrogen isotopes bulk diffusion towards the surface and the recombination at the bulk-surface interface may help improving the proper estimation of dynamic wall outgassing i.e. the modeling of fuel recycling at plasma facing components, upon which advanced edge plasma simulations can be developed [28,29].

Acknowledgements

This work has been carried out within the framework of the French Federation for Magnetic Fusion Studies (FR-FCM) and of the EUROfusion Consortium and has received funding from the Euratom research and training programme 2014-2018 and 2019-2020 under grant agreement No 633053. Work performed under EUROfusion WP PFC. The views and opinions expressed herein do not necessarily reflect those of the European Commission. The project leading to this publication has also received funding from the Excellence

Initiative of Aix-Marseille University – A*Midex, a French "Investissements d'Avenir" programme as well as from the ANR under grant ANR-18-CE05-12.

References

[1] Koyanagi T, Kumar N A P K, Hwang T, Garrison L M, Hu X, Snead L L and Katoh Y 2017 Microstructural evolution of pure tungsten neutron irradiated with a mixed energy spectrum *J. Nucl. Mater.* **490** 66–74

[2] Marian J, Becquart C S, Domain C, Dudarev S L, Gilbert M R, Kurtz R J, Mason D R, Nordlund K, Sand A E, Snead L L, Suzudo T and Wirth B D 2017 Recent advances in modeling and simulation of the exposure and response of tungsten to fusion energy conditions *Nucl. Fusion* **57** 092008

[3] Bernard E, Sakamoto R, Hodille E, Kreter A, Autissier E, Barthe M-F, Desgardin P, Schwarz-Selinger T, Burwitz V, Feuillastre S, Garcia-Argote S, Pieters G, Rousseau B, Ialovega M, Bisson R, Ghiorghiu F, Corr C, Thompson M, Doerner R, Markelj S, Yamada H, Yoshida N and Grisolia C 2019 Tritium retention in W plasma-facing materials: Impact of the material structure and helium irradiation *Nucl. Mater. Energy* **19** 403–10

[4] Dürrschnabel M, Klimenkov M, Jäntsch U, Rieth M, Schneider H C and Terentyev D 2021 New insights into microstructure of neutron-irradiated tungsten *Sci. Rep.* **11** 7572

[5] Markelj S, Schwarz-Selinger T, Pečovnik M, Založnik A, Kelemen M, Čadež I, Bauer J, Pelicon P, Chromiński W and Ciupinski L 2019 Displacement damage stabilization by hydrogen presence under simultaneous W ion damage and D ion exposure *Nucl. Fusion* **59** 086050

[6] Ialovega M, Bernard E, Bisson R, Martin C, Sakamoto R, Kreter A, Hodille E, Angot T and Grisolia C 2020 Hydrogen trapping in tungsten: impact of helium irradiation and thermal cycling *Phys. Scr.* **T171** 014066

[7] Causey R A 2002 Hydrogen isotope retention and recycling in fusion reactor plasma-facing components *J. Nucl. Mater.* **300** 91–117

[8] 't Hoen M H J, Mayer M, Kleyn A W and Zeijlmans van Emmichoven P A 2013 Strongly Reduced Penetration of Atomic Deuterium in Radiation-Damaged Tungsten *Phys. Rev. Lett.* **111** 225001

[9] Kong X-S, You Y-W, Fang Q F, Liu C S, Chen J-L, Luo G-N, Pan B C and Wang Z 2013 The role of impurity oxygen in hydrogen bubble nucleation in tungsten *J. Nucl. Mater.* **433** 357–63

[10] Hodille E A, Ghiorghiu F, Addab Y, Založnik A, Minissale M, Piazza Z, Martin C, Angot T, L. Gallais, Barthe M-F, Becquart C S, Markelj S, Mougenot J, Grisolia C and Bisson R 2017 Retention and release of hydrogen isotopes in tungsten plasma-facing components: the role of grain boundaries and the native oxide layer from a joint experiment-simulation integrated approach *Nucl. Fusion* **57** 076019

[11] Bisson R, Markelj S, Mourey O, Ghiorghiu F, Achkasov K, Layet J-M, Roubin P, Cartry G, Grisolia C and Angot T 2015 Dynamic fuel retention in tokamak wall materials: An in situ laboratory study of deuterium release from polycrystalline tungsten at room temperature *J. Nucl. Mater.* **467** 432–8

[12] Ghiorghiu F, Minissale M, Hodille E A, Grisolia C, Angot T and Bisson R 2019 Comparison of dynamic deuterium retention in single-crystal and poly-crystals of tungsten: The role of natural defects *Nucl. Instrum. Methods Phys. Res. Sect. B Beam Interact. Mater. At.* **461** 159–65

[13] Kremer K, Schwarz-Selinger T and Jacob W 2021 Influence of thin tungsten oxide films on hydrogen isotope uptake and retention in tungsten – Evidence for permeation barrier effect *Nucl. Mater. Energy* **27** 100991

[14] Ogorodnikova O V, Roth J and Mayer M 2003 Deuterium retention in tungsten in dependence of the surface conditions *J. Nucl. Mater.* **313–316** 469–77

[15] Matsunami N, Ohno N and Tokitani M 2009 Deuterium retention in tungsten oxide under low energy D2+ plasma exposure *J. Nucl. Mater.* **390–391** 693–5

[16] Minissale M, Faure J-B, Dunand A, Angot T, De Temmerman G and Bisson R 2020 Sticking Probability of Ammonia Molecules on Tungsten and 316L Stainless Steel Surfaces *J. Phys. Chem. C* **124** 17566–77

[17] Pardanaud C, Dellasega D, Passoni M, Martin C, Roubin P, Addab Y, Arnas C, Couedel L, Minissale M, Salomon E, Giacometti G, Merlen A, Bernard E, Mateus R, Alves E, Siketic Z, Radović I B and Hakola A 2020 Post-mortem analysis of tungsten plasma facing components in tokamaks: Raman microscopy measurements on compact, porous oxide and nitride films and nanoparticles *Nucl. Fusion* **60** 086004

[18] Zakeri Kh, Peixoto T R F, Zhang Y, Prokop J and Kirschner J 2010 On the preparation of clean tungsten single crystals *Surf. Sci.* **604** L1–3

[19] Rettner C T, DeLouise L A and Auerbach D J 1986 Effect of incidence kinetic energy and surface coverage on the dissociative chemisorption of oxygen on W(110) *J. Chem. Phys.* **85** 1131–49

[20] Wu P K, Tringides M C and Lagally M G 1989 Ordering kinetics of a chemisorbed overlayer: O/W(110) *Phys. Rev. B* **39** 7595–610

[21] Johnson K E, Wilson R J and Chiang S 1993 Effects of adsorption site and surface stress on ordered structures of oxygen adsorbed on W(110) *Phys. Rev. Lett.* **71** 1055–8

[22] Tamm P W and Schmidt L D 1971 Binding States of Hydrogen on Tungsten *J. Chem. Phys.* **54** 4775

[23] Wilgocka-Ślęzak D, Giela T, Freindl K, Spiridis N and Korecki J 2020 High-temperature oxygen monolayer structures on W(110) revisited *Appl. Surf. Sci.* **528** 146712

[24] Whitten J E and Gomer R 1998 The coadsorption of H and O on the W(110) plane *Surf. Sci.* **409** 16–26

[25] Nojima A and Yamashita K 2007 A theoretical study of hydrogen adsorption and diffusion on a W(1 1 0) surface *Surf. Sci.* **601** 3003–11

https://doi.org/10.1088/1741-4326/ac583a

[26] Piazza Z A, Ajmalghan M, Kolasinski R D and Ferro Y 2020 A density functional theory based thermodynamic model of hydrogen coverage on the W(110) surface *Phys. Scr.* **T171** 014025
[27] Stöhr M, Podloucky R and Müller S 2009 Ab initiophase diagram of oxygen adsorption on W(110) *J. Phys. Condens. Matter* **21** 134017
[28] Denis J, Bucalossi J, Ciraolo G, Hodille E A, Pégourié B, Bufferand H, Grisolia C, Loarer T, Marandet Y and Serre E 2019 Dynamic modelling of local fuel inventory and desorption in the whole tokamak vacuum vessel for auto-consistent plasma-wall interaction simulations *Nucl. Mater. Energy* **19** 550–7
[29] Smirnov R D, Krasheninnikov S I and Umansky M V 2020 Time-dependent modeling of coupled plasma-wall dynamics *Phys. Plasmas* **27** 032503